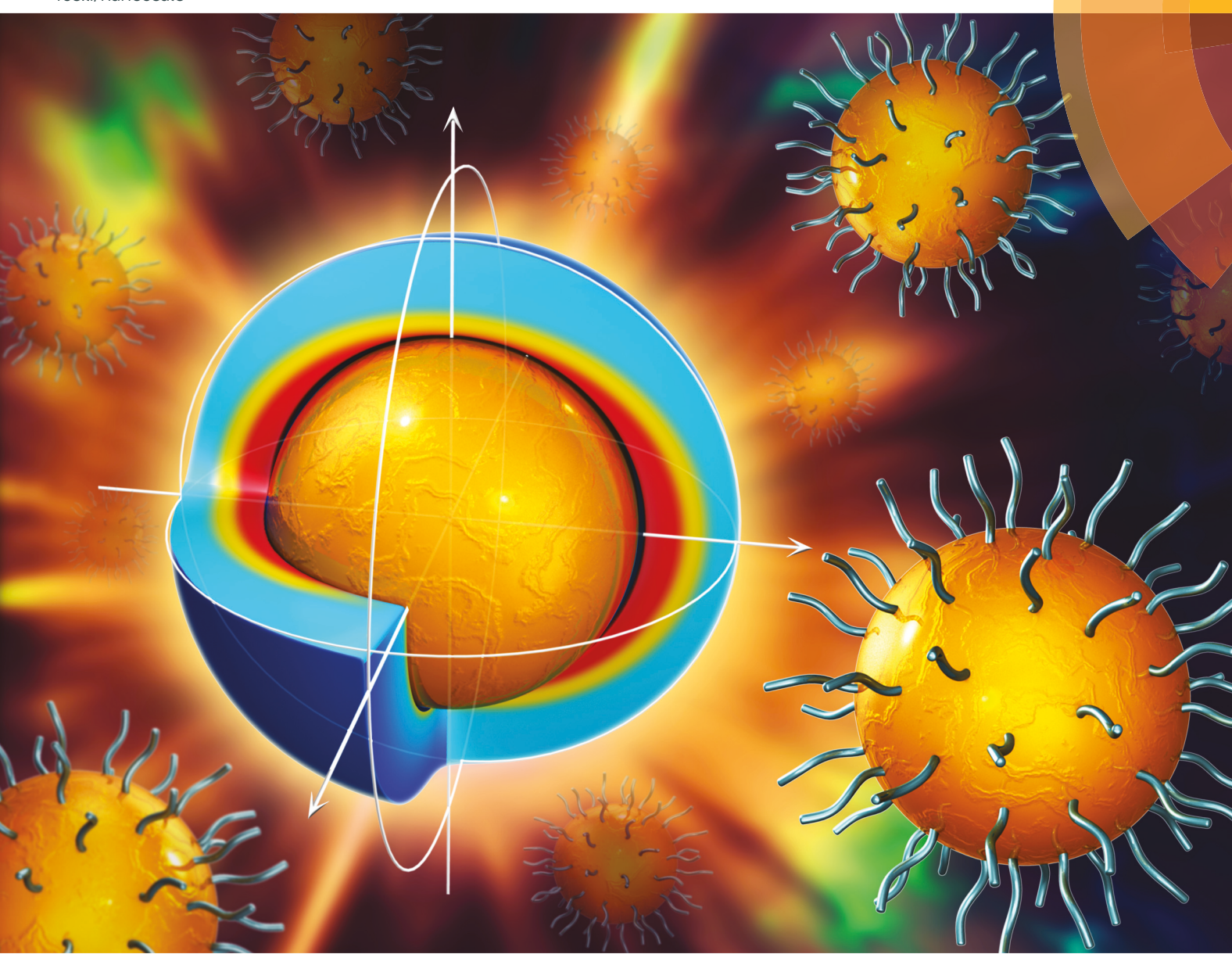
rsc.li/nanoscale



ISSN 2040-3372



#### PAPER





PAPER

View Article Online
View Journal | View Issue



Cite this: Nanoscale, 2018, 10, 22750

## An integrated experimental and theoretical study on the optical properties of uniform hairy noble metal nanoparticles†

Di Yang, ‡<sup>a</sup> Yihuang Chen, ‡<sup>b</sup> Hongshang Peng, <sup>a</sup> Gengxiang Chen <sup>a</sup> and Zhigun Lin <sup>b</sup> \*<sup>b</sup>

We report a viable route to plasmonic nanoparticles with well-controlled sizes, shapes, and compositions. A series of monodisperse Ag and Au nanoparticles capped with polystyrene chains (i.e., "hairy" nanoparticles) are crafted by capitalizing on star-like diblock copolymers as nanoreactors. Such monodisperse nanoparticles render an accurate absorption spectrum, providing a strong basis for theoretical investigation into their optical properties. By combining the experimental study with the three-dimensional finite element calculation of electromagnetic field distributions, the contributions of both intra-band and inter-band transitions to plasmonic absorption are revealed. The calculated absorption spectra perfectly reproduce the experimental observations, including the peak positions, shapes, and trends of peak shifting or broadening as a function of nanoparticle sizes. The influences of nanoparticle dimensions and surface ligands on plasmonic absorption of metallic nanoparticles are also systematically explored.

Received 1st September 2018, Accepted 1st October 2018 DOI: 10.1039/c8nr07115b

rsc.li/nanoscale

## 1. Introduction

Colloidal noble metal nanoparticles (i.e., Ag and Au) exhibit intriguing optical properties due to strong surface plasmon resonance (SPR) at optical frequencies 1-3 for a wide range of applications in surface-enhanced sensing and spectroscopy, 4,5 high-resolution imaging,6 light localization and guiding,7 photocatalysis,3,8 transport and storage of energy,9-11 and optical force enhancement in nanoaggregates.<sup>12</sup> Interestingly, the physical and chemical properties of plasmonic nanoparticles consisting of a few hundred up to several thousand atoms can be perfectly regulated by geometric and compositional engineering during synthesis to meet the requirements of relevant applications, for example, as building blocks for functional materials and devices. 13-17 Recently, a controllable preparative strategy to precisely tailor the dimension and composition of plasmonic nanoparticles with high stability has been a topic of general interest. The traditional solution-based colloidal synthesis has been widely used to produce plasmonic nanoparticles. 18 Surface passivation of nanoparticles with ligands (e.g., small molecular surfactants and linear polymers)

during their synthesis is an indispensable procedure in preventing them from agglomeration. However, the ligands tend to dissociate from the nanoparticle surface if the experimental conditions (e.g., pH, temperature, UV irradiation, etc.) are changed. Thus, incomplete and uncontrollable surface coverage or nonuniformity of polymers on the nanoparticle surface occurs, leading to the inhomogeneity of nanoparticles. Recently, nanoparticles have been prepared by using conventional micelles from the self-assembly of linear amphiphilic block copolymers.19 However, it is difficult to maintain the shape as the characteristics of the micelles for a given system depend heavily on temperature, solvent properties, etc. 20,21 To this end, we have recently developed a facile strategy for creating high-quality plasmonic nanoparticles by judiciously exploiting amphiphilic starlike copolymers with well-defined molecular architectures and molecular weights as nanoreactors. 15,22,23 In stark contrast to the conventional method for synthesizing nanoparticles capped with small ligands via relatively weak interactions, nanoparticles produced via the amphiphilic star-like copolymer strategy are intimately and permanently capped with a layer of polymer chains, resulting in excellent solubility in nonpolar solvents with prolonged stability. Moreover, the dimensions and compositions of monodisperse nanoparticles can be easily adjusted by tailoring the molecular weights of the polymer template and choosing suitable precursors for inorganic synthesis, respectively.

Over the past few decades, theoretical investigation into the SPR of plasmonic nanoparticles has been actively invoked to

<sup>&</sup>lt;sup>a</sup>School of Science, Minzu University of China, Beijing 100081, China

<sup>&</sup>lt;sup>b</sup>School of Materials Science and Engineering, Georgia Institute of Technology, Atlanta, GA 30332, USA. E-mail: zhiqun.lin@mse.gatech.edu

 $<sup>\</sup>dagger\,\text{Electronic}$  supplementary information (ESI) available. See DOI: 10.1039/c8nr07115b

<sup>‡</sup>Equal contribution.

provide better guidance to an experimental study.<sup>24-30</sup> However, some factors affecting the SPR of plasmonic nanoparticles have not yet been fully understood and often been neglected in simulation. This is mainly reflected by a large discrepancy between the calculated and experimental plasmonic absorptions. It is well-known that the existence of SPR is due to the coupling of electromagnetic waves to the motion of electrons. However, when characterizing the SPR of plasmonic nanoparticles, only transition motions of free electrons within an energy band, called intra-band excitation, are usually considered, while the influence of inter-band excitation is ignored (see the ESI† for intra-band excitation and inter-band excitation). 31-33 Recently, the effect of inter-band oscillations in the nonlinear optics of plasmonic nanocomposites has received much attention. 34,35 For instance, the metal-sapphire nanostructure was reported to enhance the incident laser field by means of SPR in which the inter- and intra-band oscillations of electrons are supposed to be involved, triggering plasmonic high-harmonic generation directly.<sup>35</sup> Notably, the contributions of the inter- and intra-band transitions to the plasmonic absorption of plasmonic nanoparticles have been theoretically investigated in several reports, 36 yet there's a lack of experimental support.

Herein, we report the crafting of a series of monodisperse Ag and Au nanoparticles by exploiting amphiphilic nonlinear block copolymers as nanoreactors, and subsequent scrutiny of the effects of the intra- and inter-band transitions on the SPR of these monodisperse plasmonic nanoparticles. The correlation between the nanoparticle sizes and the corresponding plasmonic absorptions is demonstrated experimentally. Moreover, the environment-dependence of plasmonic absorption is studied via rationally varying the surface ligands situated on the surface of plasmonic nanoparticles. As the experimental results are derived from monodisperse plasmonic nanoparticles, they provide good feedback for theoretical investigation into the SPR of plasmonic nanoparticles. Thus, by combining the systematically measured absorption spectra of plasmonic nanoparticles with the simulated absorption spectra calculated by the 3-dimensional finite element method, the influences of the intra- and inter-band transitions on their SPR are explored. More importantly, an integrated experiment and modelling study reveals the influences of dimensions and surface ligands of Ag and Au nanoparticles on the plasmonic absorption.

#### **Experimental section** 2.

### Synthesis of PS-capped Au and Ag nanoparticles

A series of monodisperse Ag and Au nanoparticles capped with polystyrene chains (i.e., hairy nanoparticles) were crafted by capitalizing on amphiphilic star-like poly(acrylic acid)block-polystyrene (PAA-b-PS) diblock copolymers as nanoreactors based on our previous work.23 The key to precisely control the diameter and shape of Ag and Au nanoparticles is

the rational design and synthesis of PAA-b-PS diblock copolymers with well-defined molecular weights and narrow molecular weight distributions. 22,23 First, heptakis[2,3,6-tri-O-(2bromo-2-methylpropionyl)]-β-cyclodextrin (denoted as 21Brβ-CD) was prepared. 23,37 A star-like PAA-b-PS diblock copolymer was then synthesized by atom transfer radical polymerization (ATRP) of tert-butyl acrylate and styrene in sequence using 21Br-β-CD as the macroinitiator, followed by hydrolysis using trifluoroacetic acid.23 Using star-like PAA-b-PS diblock copolymers as nanoreactors in a 10 ml mixed solvent containing dimethylformamide (DMF) and benzyl alcohol (BA) in the 9:1 ratio by volume, PS-capped noble metal nanoparticles were obtained with suitable precursors (i.e., AgNO<sub>3</sub> for Ag nanoparticles and  $HAuCl_4 \times 3H_2O$  for Au nanoparticles). These metallic nanoparticles were found to be highly crystalline.23

#### 2.2 Theoretical calculations

The complex dielectric function is an important parameter to express the interaction between materials and light waves. In a complex dielectric function, the contributions of the interband transition and intra-band transition can be described by the Lorentz model<sup>38</sup> and the Drude model,<sup>39</sup> respectively. Therefore, the complex dielectric function of noble metals  $\varepsilon(\omega) = \varepsilon_1(\omega) + i\varepsilon_2(\omega)$  can be separated into two contributions associated with inter-band and intra-band transitions, respectively,  $\varepsilon(\omega) = \varepsilon_{\text{interband}}(\omega) + \varepsilon_{\text{intraband}}(\omega)$ . The contribution of the inter-band transition to the dielectric function is described by the simple semi-quantum model, resembling the Lorentz model:38

$$\varepsilon_{\rm interband}(\omega) = \sum_{j=1}^{N} \frac{f_j \Omega_{\rm p}^{\ 2}}{\omega_j^{\ 2} - \omega^2 - {\rm i}\omega\gamma_j} \eqno(1)$$

where  $\Omega_p$  denotes the plasma frequency associated with the inter-band transition, and N is the number of resonances with the frequency  $\omega_i$ , strength  $f_i$ , and damping constant  $\gamma_i$ . These parameters for Ag and Au used here are obtained from the report in which metallic optical parameters were obtained on the basis of the measured spectra of metallic films.<sup>38</sup> The contribution of the intra-band transition to the dielectric function can be derived using the Drude model.<sup>39</sup> Since the particle size of metallic nanoparticles is comparable to the mean free path of free-electrons, the finite size effect needs to be taken into account. The modification of the finite size effect in the dielectric function is achieved by increasing a size-dependent factor  $\frac{AV_{\mathrm{f}}}{L_{\mathrm{eff}}}$  to the bulk damping rate of free-electron  $\gamma_{\mathrm{D0}}$ . Consequently, the modified damping rate of the free-electron is given by  $\gamma = \gamma_{D0} + \frac{AV_{\mathrm{f}}}{L_{\mathrm{eff}}}$ , where  $V_{\mathrm{f}}$  is the Fermi velocity of the electron,  $L_{\text{eff}}$  the effective mean free path of the electron, and A the proportionality factor.  $L_{\text{eff}}$  depends on the size and shape of nanoparticles and can be calculated for different shaped nanoparticles using  $L_{\text{eff}} = 4V/S$ , where V and S are the volume

**Paper** Nanoscale

and surface area of nanoparticles, respectively. The modified Drude model is given as follows:40

$$\begin{split} \varepsilon_{\rm intraband} &= 1 - \frac{\omega_{\rm p}^2}{\omega^2 + \mathrm{i}\omega \left(\gamma_{\rm D0} + \frac{AV_{\rm f}}{L_{\rm eff}}\right)} \\ &= 1 - \frac{\omega_{\rm p}^2}{\omega^2 + \left(\gamma_{\rm D0} + \frac{AV_{\rm f}}{L_{\rm eff}}\right)^2} + \mathrm{i}\frac{\omega_{\rm p}^2}{\omega^3} \left[ \frac{\left(\gamma_{\rm D0} + \frac{AV_{\rm f}}{L_{\rm eff}}\right)}{\left(\gamma_{\rm D0} + \frac{AV_{\rm f}}{L_{\rm eff}}\right)^2} \right] \end{aligned} \tag{2}$$

where  $\omega_{\rm p}$  is the plasma frequency associated with the intraband transition. For Ag,  $\omega_{\rm p}, \gamma_{\rm D0},$  and  $V_{\rm f}$  are 9.04 eV, 0.02125 eV and 1.39  $\times$  10<sup>6</sup> m s<sup>-1</sup>, respectively. 41 For Au,  $\omega_p$ ,  $\gamma_{D0}$  and  $V_f$  are 8.89 eV, 0.07088 eV and  $1.40 \times 10^6$  m s<sup>-1</sup>, respectively.<sup>41</sup> The proportionality factor A corresponds to an introduction of correction to errors in  $\varepsilon_{intraband}$  and can be directly deduced by fitting the measured spectra. 42 In this study, A was set to 0.1 according to the measured spectra. In order to facilitate comparison, the A-value remained 0.1 for Ag and Au nanoparticles

with various dimensions. The relationship of  $\omega \gg \left(\gamma_{\rm D0} + \frac{AV_{\rm f}}{L_{\rm eff}}\right)$  exists at optical frequencies, and the finite size effect noted above mainly influences the imaginary part of  $\varepsilon_{\text{intraband}}$  according to eqn (2), which has also been verified in the literature. 43 Moreover, on the basis of the Kramers-Kronig relation, the real part of complex dielectric constants  $\varepsilon_1(\omega)$  changes slightly if the size of the Ag particles decreases, whereas the imaginary part  $\varepsilon_2(\omega)$ is markedly enhanced (up to tenfold the bulk value).44 Therefore, in our calculations on plasmonic nanoparticles,  $\varepsilon_1(\omega)$  was fixed to the real component of  $\varepsilon_{interband}(\omega)$  +  $\varepsilon_{\text{intraband}}(\omega)$ , while  $\varepsilon_2(\omega)$  was changed (i.e., set as the imaginary component of  $\varepsilon_{\text{intraband}}(\omega)$  or the sum of  $\varepsilon_{\text{interband}}(\omega)$  +  $\varepsilon_{\text{intraband}}(\omega)$ ) to explore the mechanism of the plasmonic absorption of metallic nanoparticles.

The extinction cross-section ( $\delta_{\text{ext}}$ ) is defined as the sum of the absorption cross-section ( $\delta_{abs}$ ) and the scattering crosssection ( $\delta_{sca}$ ). For the small-sized colloidal nanoparticles investigated in this work, the absorption dominates over the scattering by approximately 100 times, so  $\delta_{\rm sca} = \delta_{\rm abs} + \delta_{\rm sca} \approx \delta_{\rm abs}$ . The absorption cross-section ( $\delta_{abs}$ ) of nanoparticles can be obtained by integrating the absorbed power density over the entire volume (V) of the metallic part:<sup>45</sup>

$$\delta_{\text{abs}}(\omega) = \frac{2}{c\varepsilon_0} \int_{V} [\sigma(\omega) \mathbf{E} \cdot \mathbf{E}^* - i\omega \mathbf{E} \cdot \mathbf{D}^*] dV$$
 (3)

where E, D, and  $\sigma$  are the electric field intensity, electric displacement, and electrical conductivity, respectively. The 3-dimensional calculations of electromagnetic field distributions were performed by solving the Maxwell equations using the COMSOL Multiphysics (COMSOL Inc., Burlington, MA).

#### 3. Results and discussion

Fig. 1 shows the transmission electron microscopy (TEM) images of the as-prepared PS-capped Ag and Au nanoparticles. The average diameters of these uniform Ag nanoparticles are  $11.9 \pm 0.3$  nm (Fig. 1a) and  $18.1 \pm 0.5$  nm (Fig. 1b) crafted by capitalizing on two star-like PAA-b-PS diblock copolymers with

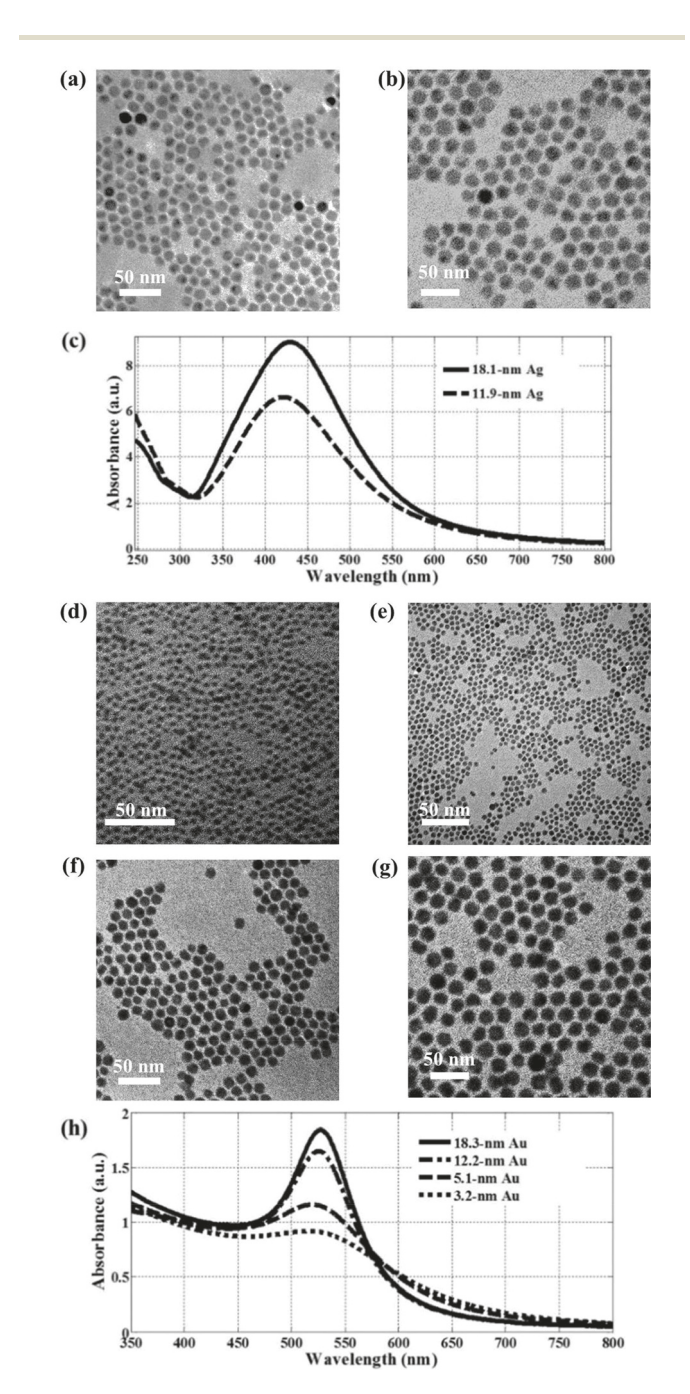


Fig. 1 TEM images of PS-capped noble metal nanoparticles using amphiphilic star-like PAA-b-PS diblock copolymers as nanoreactors. The diameters of Ag nanoparticles are (a) 11.9  $\pm$  0.3 nm and (b) 18.1  $\pm$ 0.5 nm, whereas the diameters of Au nanoparticles are (d) 3.2  $\pm$  0.1 nm, (e)  $5.1 \pm 0.2$  nm, (f)  $12.2 \pm 0.5$  nm, and (g)  $18.3 \pm 0.4$  nm. (c) and (h) UV-Vis spectra for PS-capped Ag and Au nanoparticles, respectively.

Nanoscale Paper

different molecular weights of inner PAA blocks, respectively. Similarly, Au nanoparticles with average diameters of 3.2  $\pm$  0.1,  $5.1 \pm 0.2$ ,  $12.2 \pm 0.5$ , and  $18.3 \pm 0.4$  nm (Fig. 1d-g) were also obtained by varying the molecular weight of the inner PAA blocks of star-like PAA-b-PS diblock copolymers. It is noteworthy that the standard deviations of these nanoparticles are all within 5% of their average diameter, signifying that they are monodisperse. The plasmonic absorption of these uniform nanoparticles in toluene was scrutinized by UV-vis absorption spectroscopy measurements, as shown in Fig. 1c and h, respectively. Several clear trends can be found by comparing the absorption spectra: (i) the plasmonic absorption peak shifted to the shorter wavelength with a decrease of the metal nanoparticle diameter. Specifically, the absorption maximum of Ag nanoparticles shifts from 429 nm to 423 nm as the diameter decreases from 18.1 nm to 11.9 nm. Similarly, the peak positions of Au nanoparticles decrease linearly from 527 to 516 nm with the decrease of diameter from 18.3 to 3.2 nm. (ii) As the diameter of metallic nanoparticles decreases, the fullwidth-at-half-maximum (FWHM) of the plasmonic absorption spectra increases. In the case of Au nanoparticles, the FWHM increases from 51 nm to 62 nm as the diameter decreases from 18.3 nm to 3.2 nm. (iii) Compared with Au nanoparticles, Ag nanoparticles possess a more obvious plasmonic absorption peak in the visible region due to a distinct valley at approximately 315 nm separating the visible absorption from the ultraviolet absorption. Furthermore, we studied the effect of ligands (i.e., PS chains and small molecules oleylamine) attached to the nanoparticle surface on the plasmonic absorption of metallic nanoparticles. Fig. 2 compares the UV-vis spectra of 18 nm PS-capped Au nanoparticles and oleylaminecapped Au nanoparticles. In comparison with oleylaminecapped Au nanoparticles, the UV-vis spectral peak of PScapped Au nanoparticles shifts to the longer wavelength.

In order to gain insights into the above trends of the plasmonic absorptions and effects of the intra- and inter-band transitions on the SPR of plasmonic nanoparticles, we calculated the absorption cross-sections of plasmonic nanoparticles via the 3-dimensional calculation of electromagnetic field distribution. On the basis of morphologies of the as-synthesized nanoparticles, a detailed geometric model was created to represent PS-capped noble metal nanoparticles in toluene, as shown in Fig. 3a. We note that the refractive indices of toluene and the PS-layer were from the literature. 46 The computational

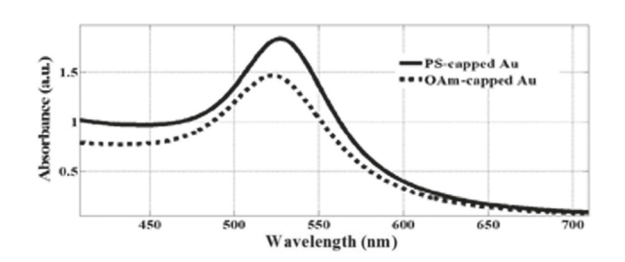
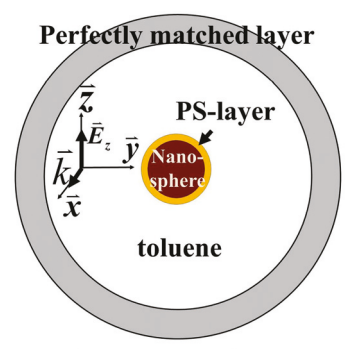
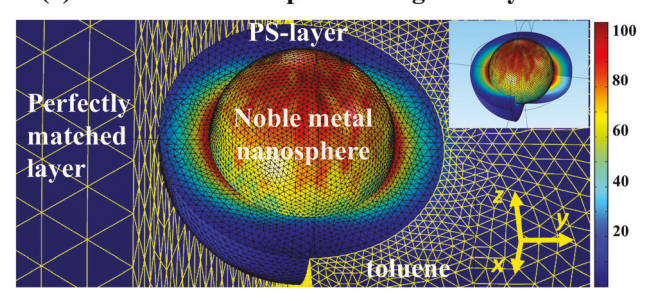


Fig. 2 UV-vis spectra of 18 nm PS-capped Au nanoparticles and 18 nm oleylamine-capped Au nanoparticles.



## (a) Cross section computational geometry



## (b) Distributions of meshes and the electric field

Fig. 3 (a) A cross-section of the computational geometry. The calculation dimension is truncated by a perfectly matched layer, which is placed sufficiently far from the nanoparticle. The incident wave is polarized along the z axis, traveling along the x axis.  $\overrightarrow{E_z}$  and  $\overrightarrow{k}$  are the incident electric field and the wave vector, respectively. The medium inside is toluene. The metallic nanoparticle is cladded by a 4 nm PS-layer. (b) Plots of the relative electric field,  $E = (E \cdot E^*)^{1/2} / |E_{inc}|$ , where  $(E \cdot E^*)^{1/2}$  is the amplitude of the total electric field and  $|E_{inc}| = 1 \text{ J nm}^{-2}$  is the amplitude of the incident field. The Au nanoparticle shown is 18 nm in diameter cladded by a 4 nm PS-layer. The view angle is shown by a 3D coordinate on the bottom right. The inset on the top right shows the electric field surrounding the nanoparticle on both xy and yz planes.

domain was artificially truncated by the perfectly matched layer (PLM) originally formulated by Berenger, 47 which can strongly absorb the outgoing waves from the interior of a computational region without reflecting them back into the interior. In addition, the PML was placed sufficiently far from the nanoparticle in order to minimize the effect of this artificial boundary. Fig. 3b provides an example of 3-dimensional mesh discretization of the model and the electric field around the nanoparticle. Meshing was performed with tetrahedral elements. Considering the characteristic of a local electromagnetic field distribution of noble metal nanoparticles, a gradual meshing method was used in the calculation, that is, the mesh around the nanoparticle was extremely finer than the mesh far away from the nanoparticle.

The plasmonic absorption of visible light of Ag and Au nanoparticles has been recognized due to the intra-band transitions of free-electrons, 48 to which our theoretical calculations have afforded convincing evidence.  $\varepsilon_2(\omega)$  was first set as the imaginary component of  $\varepsilon_{\mathrm{intraband}}(\omega)$  without considering the contribution of the inter-band transitions. The electromagnetic field calculations were carried out using the finite

Paper Nanoscale

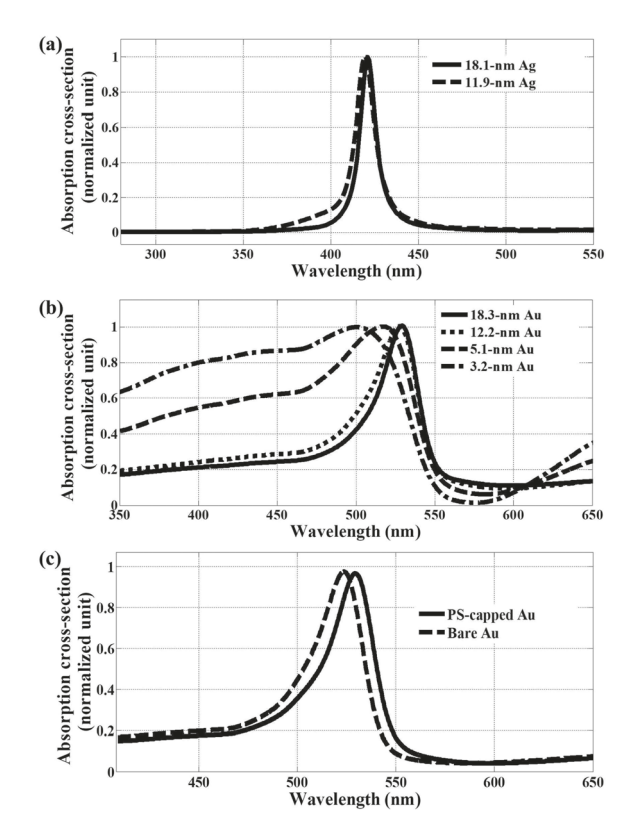


Fig. 4 The simulated absorption cross-sections of (a) PS-capped Ag nanoparticles with diameters of 11.9 and 18.1 nm, (b) PS-capped Au nanoparticles with diameters of 3.2, 5.1, 12.2, and 18.3 nm, and (c) 18 nm Au nanoparticles capped with PS or oleylamine (*i.e.*, bare Au). The value of  $\varepsilon_2(\omega)$  equaled the imaginary component of  $\varepsilon_{\text{intraband}}(\omega)$ .

element method. Fig. 4a and b show the absorption cross-sections of the PS-capped Ag and Au nanoparticles, respectively. The peak intensities were normalized for comparison. Obviously, the peak positions and the trends of peak blueshifting and broadening with the decreased nanoparticle sizes are consistent with that of the measured spectra shown in Fig. 1. Moreover, the influence of the cladding (capping) of Au nanoparticles on the plasmonic absorption peak was investigated by the numerical calculation based on  $\varepsilon_{\text{intraband}}(\omega)$ . The oleylamine-capped Au nanoparticles were regarded as bare Au nanoparticles in simulation owing to the negligible influence of oleylamine on the optical field. 49,50 Fig. 4c shows a comparison between the simulated absorption cross-section of PScapped Au nanoparticles and that of bare Au nanoparticles. The simulated absorption peak of the PS-capped Au nanoparticles shifts to the longer wavelength, which is consistent with the measured spectra (Fig. 2). On the other hand, with regard to the inter-band transition, the reported resonance frequencies of Ag films expressed by wavelengths using 1240/frequency (eV) are 1519.4, 276.7, 151.5, 136.5, 061.1 nm and that of Au films are 2987.6, 1493.8, 417.6, 288.1, 93.1 nm.<sup>38</sup> These wavelengths are far away from the measured plasmonic absorption peaks in the visible region (i.e., 429 nm for 18 nm Ag and 527 nm for 18 nm Au as shown in Fig. 1). This indicates that the inter-band transition is not a major contributor to the plasmonic absorption in the visible region. Taken together, the results described above show that the plasmonic absorption of Ag and Au nanoparticles in the visible region originates from the intra-band transition of free-electrons.

It is worth noting that the amplitude of the calculated absorption cross-sections in Fig. 4 descended in the ultraviolet region, signifying that the absorption band in the ultraviolet region in the measured spectra is not due to intra-band transitions. We then set  $\varepsilon_2(\omega)$  as the imaginary component of  $\varepsilon_{\rm intraband}(\omega) + \varepsilon_{\rm interband}(\omega)$  and calculated the absorption crosssections of the PS-capped Ag and Au nanoparticles again. The calculations are shown in Fig. 5. Intriguingly, exactly as in the measured spectra, the absorption intensity in the ultraviolet region enhances in the calculated absorption cross-sections. Therefore, the inter-band transition is a major contributor to the spectral absorption in the ultraviolet region. Meanwhile, it is noticeable that when the reported resonance frequencies  $\omega_i$ (in eqn (1)) derived from Ag and Au films<sup>38</sup> were utilized as that of Ag and Au nanoparticles, respectively, the simulated absorption intensities of both in the ultraviolet region were much higher than the measured ones, illustrated by the dotted curves in Fig. 5a and b, respectively. The inter-band transition with frequency closest to the visible frequency has a great influence on the plasmonic absorption peak in the visible region. For Ag, the reported inter-band transition closest to the plasmonic absorption peak of the visible region is at around 276.7 nm (i.e., 4.481 eV denoted by  $\omega_{1Ag}$ ), approximately 153 nm away from the plasmonic absorption peak at 427 nm. For Au, on the other hand, the closest inter-band transition to the visible region was reported at 417.6 nm (i.e., 2.969 eV denoted by  $\omega_{1Au}$ ), approximately 109 nm away from the plasmonic absorption peak at 527 nm. Clearly, compared with Au, the inter-band transition of Ag has less influence on the plasmonic absorption in the visible region. This also explains why the plasmonic absorption at optical frequencies of Ag nanoparticles is more obvious than that of Au nanoparticles. It is well-known that compared with film or bulk materials, the band gap of nanoparticles increases. Thus, the resonance frequency of the inter-band transition should shift to a higher frequency. In light of our experimental measurements, for both Ag and Au, we attempted to obtain the resonance frequencies of the inter-band transition closest to the plasmonic absorption peaks in the visible region. The resonance frequencies of the inter-band transition in Ag or Au nearest to the plasmonic absorption peak of visible light are represented by the sum of the reported resonance frequency of the Ag or Au film and the increment ( $\Delta$ ), i.e.,  $\omega_{1Ag} + \Delta$  for Ag, and  $\omega_{1Au} + \Delta$  for Au. The absorption cross-sections of Ag and Au nanoparticles with 18 nm diameter were calculated using different  $\Delta$  and were compared with the measured ones, as shown in Fig. 5a and b, respectively. As  $\Delta$  increases, the calculated absorption intensity in the ultraviolet region decreases and the valley near ultraviolet region shifts to the shorter wavelength, which is much consistent with the measured one. This indicates that the frequency of the inter-band transitions of Ag and Au nano-

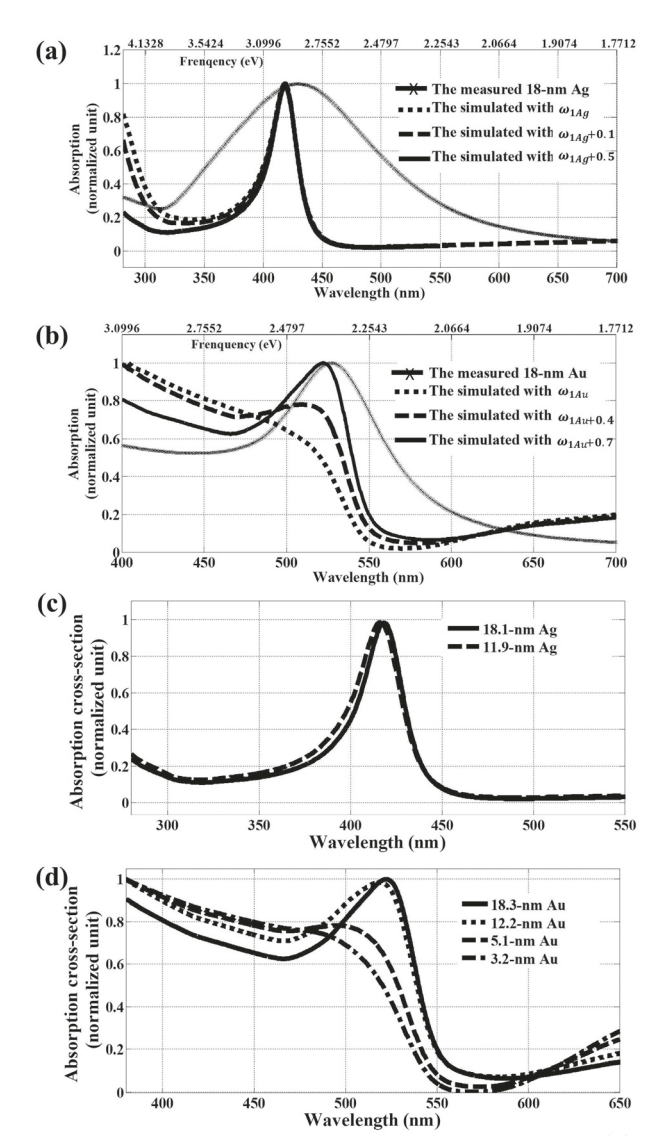


Fig. 5 Simulated absorption cross-sections according to  $\varepsilon(\omega)$  $\varepsilon_{\mathrm{intraband}}(\omega)$  +  $\varepsilon_{\mathrm{interband}}(\omega)$ : (a) 18 nm PS-capped Ag nanoparticles with the resonance frequencies of  $\omega_{\rm 1Ag}$ ,  $\omega_{\rm 1Ag}$  + 0.1 eV, and  $\omega_{\rm 1Ag}$  + 0.5 eV; (b) 18 nm PS-capped Au nanoparticles with the resonance frequencies of  $\omega_{1Au}$ ,  $\omega_{1Au}$  + 0.4 eV, and  $\omega_{1Au}$  + 0.7 eV.  $\omega_{1Ag}$  and  $\omega_{1Au}$  are the resonance frequencies of Ag and Au films, respectively, reported in the literature.<sup>38</sup> A representative experimental spectrum is also presented in both (a) and (b) for comparison. Simulated absorption cross-sections based on the optimized inter-band transition frequencies in  $\varepsilon(\omega)$ : (c) PS-capped Ag nanoparticles with diameters of 11.9 and 18.1 nm; (d) PS-capped Au nanoparticles with diameters of 3.2, 5.1, 12.2, and 18.3 nm.

particles is larger than that of Ag and Au films. Therefore, in Ag or Au nanoparticles, the influence of inter-band transitions in the ultraviolet region on the plasmonic absorption of visible light is weaker than it is in Ag or Au films.

Based on the above analysis, in  $\varepsilon_{\text{interband}}(\omega)$  the inter-band transition frequencies closest to the visible region are suggested to be 4.981 eV for Ag nanoparticles and 3.669 eV for Au nanoparticles, which are higher than the reported values (4.481 eV for the Ag film and 2.969 eV for the Au film).

According to the optimized dielectric function  $\varepsilon(\omega)$ , the absorption cross-sections of PS-capped Ag and Au nanoparticles with various sizes were calculated again, as shown in Fig. 5c and d, respectively. Clearly, from the ultraviolet to visible region, not only the peak position and the trend of peak shifting or broadening with nanoparticle sizes but also the shape of absorption curves are consistent with those of the measured spectra.

On the basis of the measured and simulated results described above, we scrutinized the size- and environmentdependence of the peak position and width of the plasmonic absorption spectra. For small enough particles, the discrete characteristics of the electronic energy levels within an energy band become obvious. The average electronic energy level spacing of successive quantum levels  $\delta E$ , known as the Kubo gap, is given by  $\delta E = 4E_f/3m$ , where  $E_f$  is the Fermi energy of the bulk material and m is the total number of electrons in a nanocrystal.<sup>51</sup> Clearly, the smaller nanoparticle has a smaller m, and thus a larger  $\delta E$ . Therefore, the absorption energies of free-electron transitions within the energy band (the sp-band for Ag and Au) are blue-shifted with decreasing nanoparticle size. Additionally, the fact that the plasmonic absorption spectrum broadens with the decreased nanoparticle sizes can be rationalized by Mie theory. 43 The full width at half maximum (FWHM,  $\Gamma$ ) is given by the phenomenological damping constant  $\gamma = \gamma_{D0} + \frac{AV_{\rm f}}{L_{\rm eff}}$  by combining Mie theory and eqn (2), *i.e.*,  $\Gamma \approx \gamma$ . 52 Obviously, the damping constant increases with a decrease of nanoparticle size due to the stronger surface scattering of free-electrons, and so does the FWHM.

Moreover, we investigated the red-shift of the plasmonic absorption peak caused by the PS-claddings of nanoparticles. It is clear that the shift trend of the simulated absorption spectra agrees with the experimental observations, as shown in Fig. 2 and 4c, respectively. As all parameters related to the Au nanoparticle including the dielectric constant, dimension, and morphology remained unchanged in simulation, the red-shift should be due to the cladding (i.e., capping) material on the Au nanoparticle surface rather than the Au nanoparticle itself. The influence of the cladding material on the plasmonic absorption peak can be elucidated as follows. As all the material parameters of an Au nanoparticle are fixed, the wavelength of light which excites the plasmonic resonance absorption of the Au nanoparticle (denoted as  $\lambda_p$ ) can be determined.

A dielectric wavelength of light is represented as  $\frac{\lambda_0}{n}$ , where  $\lambda_0$ and n are the vacuum wavelength and refractive index of the dielectric, respectively. In the toluene solution, the  $\lambda_p$  light wave induces the plasmonic resonance absorption of the Au nanoparticle, resulting in  $\frac{\lambda_0}{n_{\text{toluene}}} = \lambda_P$ , *i.e.*, the vacuum wave-

length of exciting plasmonic resonance absorption of the Au nanoparticle is  $\lambda_0 = n_{\text{toluene}} \cdot \lambda_p$ . Similarly, in the cladding of PS dielectric, the vacuum wavelength to excite plasmonic resonance absorption of the Au nanoparticle is  $\lambda_0 = n_{PS} \cdot \lambda_p$ . The refractive index of PS ( $n_{PS} = 1.59$ ) is larger than that of toluene **Paper** 

 $(n_{\text{toluene}} = 1.49)$ . Consequently, as the vacuum wavelength is an independent variable, a red-shift of the absorption peak of the PS-capped Au nanoparticle was thus observed. Such a characteristic of the plasmonic absorption of a noble metal may be applied for an accurate measurement of the refractive index of a medium.

#### Conclusion 4.

In summary, monodisperse Ag and Au nanoparticles with different diameters were synthesized using amphiphilic star-like diblock copolymers as nanoreactors. On the basis of the experimentally measured plasmonic absorption spectra of synthesized Ag and Au nanoparticles, 3-dimensional finite element calculation was performed. The calculated absorption spectra well reproduced the experimental observations. By combining the experiments and 3-dimensional finite element calculations, the contribution of intra-band transitions and inter-band transitions to the plasmonic absorption of Ag and Au nanoparticles was scrutinized. The intra- and inter-band transitions were found to contribute primarily to the visible and ultraviolet absorption spectra, respectively. Meanwhile, the influences of nanoparticle sizes and surface ligands on the plasmonic absorption were systematically investigated. As the diameter of metallic nanoparticles decreased, the plasmonic absorption peak shifted to a shorter wavelength, whereas the FWHM increased. In addition, PS chains tethered on the metal nanoparticle surface caused a red-shift of the plasmonic absorption peak. Such experimentally observed size- and environment-dependence of the peak position and width of the plasmonic absorption spectra was also investigated theoretically.

## Conflicts of interest

There are no conflicts to declare.

## Acknowledgements

We gratefully acknowledge funding support from the National Science Foundation (CMMI 1562075 and 1727313; DMR 1709420), the Air Force Office of Scientific Research (FA9550-16-1-0187), the National Science Foundation of China (61875234, 61775245 and 61627814), and the National Study Fund Committee (Project number: 2016-QT-049).

## References

- 1 N. G. Bastus, J. Piella and V. Puntes, Langmuir, 2016, 32, 290.
- 2 B. Dastmalchi, P. Tassin, T. Koschny and C. M. Soukoulis, Adv. Opt. Mater., 2016, 4, 177.
- 3 A. Zaleska-Medynska, M. Marchelek, M. Diak and E. Grabowska, Adv. Colloid Interface Sci., 2016, 229, 80.

- 4 S. Zaleski, A. J. Wilson, M. Mattei, X. Chen, G. Goubert, M. F. Cardinal, K. A. Willets and R. P. Van Duyne, Acc. Chem. Res., 2016, 49, 2023.
- 5 G. Haran, Acc. Chem. Res., 2010, 43, 1135.
- 6 W. Wang, S. Wang, Q. Liu, J. Wu and N. Tao, Langmuir, 2012, 28, 13373.
- 7 Y. Zhang, C. Gu, A. M. Schwartzberg, S. Chen and J. Z. Zhang, Phys. Rev. B: Condens. Matter Mater. Phys., 2006, 73, 165405.
- 8 W. L. Ong, M. Gao and G. W. Ho, Nanoscale, 2013, 5,
- 9 E. Ozbay, Science, 2006, 311, 189.
- 10 C. F. Tan, W. L. Ong and G. W. Ho, ACS Nano, 2015, 9, 7661.
- 11 M. Gao, P. K. N. Connor and G. W. Ho, Energy Environ. Sci., 2016, 9, 3151.
- 12 H. Xu and M. Käll, Phys. Rev. Lett., 2002, 89, 246802.
- 13 M. Baghbanzadeh, L. Carbone, P. D. Cozzoli and C. O. Kappe, Angew. Chem., Int. Ed., 2011, 50, 11312.
- 14 M. T. Sheldon, J. van de Groep, A. M. Brown, A. Polman and H. A. Atwater, Science, 2014, 346, 828.
- 15 Y. Chen, D. Yang, Y. J. Yoon, X. Pang, Z. Wang, J. Jung, Y. He, Y. W. Harn, M. He, S. Zhang, G. Zhang and Z. Lin, J. Am. Chem. Soc., 2017, 139, 12956.
- 16 J. Xiao and L. Oi, Nanoscale, 2011, 3, 1383.
- 17 S. Linic, P. Christopher, H. Xin and A. Marimuthu, Acc. Chem. Res., 2013, 46, 1890.
- 18 J. Park, J. Joo, S. G. Kwon, Y. Jang and T. Hyeon, Angew. Chem., Int. Ed., 2007, 46, 4630.
- 19 W. L. Leong, P. S. Lee, A. Lohani, Y. M. Lam, T. Chen, S. Zhang, A. G. Dodabalapur and S. Mhaisalkar, Adv. Mater., 2008, 20, 2325.
- 20 S. B. Darling, Prog. Polym. Sci., 2007, 32, 1152.
- 21 J. Rodríguez-Hernández, F. Chécot, Y. Gnanou and S. Lecommandoux, Prog. Polym. Sci., 2005, 30, 691.
- 22 X. Pang, L. Zhao, W. Han, X. Xin and Z. Lin, Nat. Nanotechnol., 2013, 8, 426.
- 23 Y. Chen, Y. J. Yoon, X. Pang, Y. He, J. Jung, C. Feng, G. Zhang and Z. Lin, Small, 2016, 12, 6714.
- 24 A. Christ, T. Zentgraf, J. Kuhl, S. G. Tikhodeev, N. A. Gippius and H. Giessen, Phys. Rev. B: Condens. Matter Mater. Phys., 2004, 70, 125113.
- 25 B. Grześkiewicz, K. Ptaszyński and M. Kotkowiak, Plasmonics, 2014, 9, 607.
- 26 S. Maegawa, H. Matsuoka, S. Fukui, F. Itoigawa and T. Nakamura, Tribol. Lett., 2016, 64, 7.
- 27 G. V. Hartland, Chem. Rev., 2011, 111, 3858.
- 28 L. Yadgarov, C. L. Choi, A. Sedova, A. Cohen, R. Rosentsveig, O. Bar-Elli, D. Oron, H. Dai and R. Tenne, ACS Nano, 2014, 8, 3575.
- 29 Y. R. Davletshin, A. Lombardi, M. F. Cardinal, V. Juvé, A. Crut, P. Maioli, L. M. Liz-Marzán, F. Vallée, N. D. Fatti and J. C. Kumaradas, ACS Nano, 2012, 6, 8183.
- 30 D. Yang, X. Pang, Y. He, Y. Wang, G. Chen, W. Wang and Z. Lin, Angew. Chem., Int. Ed., 2015, 54, 12091.
- 31 P. C. Ray, Chem. Rev., 2010, 110, 5332.

32 S. Mazzucco, N. Geuquet, J. Ye, O. Stéphan, W. V. Roy, 42 H. E

- 32 S. Mazzucco, N. Geuquet, J. Ye, O. Stéphan, W. V. Roy, P. V. Dorpe, L. Henrard and M. Kociak, *Nano Lett.*, 2012, 12, 1288.
- 33 A. Siabi-Garjan and H. Savaloni, Plasmonics, 2015, 10, 1.
- 34 R. C. Fernándezhernández, R. Gleasonvillagran, C. Torrestorres, L. Rodríguezfernández, A. Crespososa, J. C. Cheangwong, A. Lópezsuárez, R. Rangelrojo, A. Oliver and J. A. Reyesesqueda, J. Opt., 2012, 14, 125203.
- 35 S. Han, H. Kim, Y. W. Kim, Y.-J. Kim, S. Kim, I.-Y. Park and S.-W. Kim, *Nat. Commun.*, 2016, 7, 13105.
- 36 A. O. Govorov, H. Zhang, H. V. Demir and Y. K. Gun'Ko, Nano Today, 2014, 9, 85.
- 37 Y. Chen, Z. Wang, Y. He, Y. J. Yoon, J. Jung, G. Zhang and Z. Lin, *Proc. Natl. Acad. Sci. U. S. A.*, 2018, **115**, E1391.
- 38 A. D. Rakić, A. B. Djurišić, J. M. Elazar and M. L. Majewski, *Appl. Opt.*, 1998, 37, 5271.
- 39 P. Drude, Ann. Phys., 2006, 308, 369.

Nanoscale

- 40 U. Kreibig and M. Vollmer, in *Optical Properties of metal clusters*, Springer-Verlag Berlin Heidelberg, Germany, 1995.
- 41 E. J. Zeman and G. C. Schatz, *J. Phys. Chem. C*, 1987, **91**, 634.

- 42 H. Baida, P. Billaud, S. Marhaba, D. Christofilos, E. Cottancin, A. Crut, J. Lermé, P. Maioli, M. Pellarin, M. Broyer, N. Del Fatti, F. Vallée, A. Sánchez-Iglesias, I. Pastoriza-Santos and L. M. Liz-Marzán, *Nano Lett.*, 2009, 9, 3463.
- 43 M. Hu, C. Novo, A. Funston, H. Wang, H. Staleva, S. Zou, P. Mulvaney, Y. Xia and G. V. Hartland, *J. Mater. Chem.*, 2008, **18**, 1949.
- 44 D. P. U. Kreibig, Eur. Phys. J. A, 1970, 234, 307.
- 45 O. L. Muskens, G. Bachelier, N. D. Fatti, F. Vallée, A. Brioude, X. Jiang and M.-P. Pileni, J. Phys. Chem. C, 2008, 112, 8917.
- 46 A. Samoc, J. Appl. Phys., 2003, 94, 6167.
- 47 J.-P. Berenger, J. Comput. Phys., 1994, 114, 185.
- 48 C. Noguez, J. Phys. Chem. C, 2007, 111, 3806.
- 49 V. V. Vodnik, D. K. Božanić, E. Džunuzović, J. Vuković and J. M. Nedeljković, *Eur. Polym. J.*, 2010, **46**, 137.
- 50 M. Ochiai, Y. Nishi, S. Goto and H. J. Frohn, *Angew. Chem.*, *Int. Ed.*, 2005, **44**, 406.
- 51 U. Kreibig, J. Phys. F: Met. Phys., 2001, 4, 999.
- 52 M. Hu, C. Novo, A. Funston, H. Wang, H. Staleva, S. Zou, P. Mulvaney, Y. Xia and G. V. Hartland, *J. Mater. Chem.*, 2008, **18**, 1949.